Deficiencies in tRNA synthetase editing activity cause cardioproteinopathy

Ye Liu[a], Jakob S. Satz[a], My-Nuong Vo[b], Leslie A. Nangle[b,1], Paul Schimmel[b,c,2], and Susan L. Ackerman[a,2]

[a]Howard Hughes Medical Institute, The Jackson Laboratory, Bar Harbor, ME 04609; [b]The Skaggs Institute for Chemical Biology, The Scripps Research Institute, La Jolla, CA 92037; and [c]The Scripps Research Institute, Scripps Florida, Jupiter, FL 33458

Contributed by Paul Schimmel, October 25, 2014 (sent for review May 26, 2014)

Misfolded proteins are an emerging hallmark of cardiac diseases. Although some misfolded proteins, such as desmin, are associated with mutations in the genes encoding these disease-associated proteins, little is known regarding more general mechanisms that contribute to the generation of misfolded proteins in the heart. Reduced translational fidelity, caused by a hypomorphic mutation in the editing domain of alanyl-tRNA synthetase (AlaRS), resulted in accumulation of misfolded proteins in specific mouse neurons. By further genetic modulation of the editing activity of AlaRS, we generated mouse models with broader phenotypes, the severity of which was directly related to the degree of compromised editing. Severe disruption of the editing activity of AlaRS caused embryonic lethality, whereas an intermediate reduction in AlaRS editing efficacy resulted in ubiquitinated protein aggregates and mitochondrial defects in cardiomyocytes that were accompanied by progressive cardiac fibrosis and dysfunction. In addition, autophagic vacuoles accumulated in mutant cardiomyocytes, suggesting that autophagy is insufficient to eliminate misfolded proteins. These findings demonstrate that the pathological consequences of diminished tRNA synthetase editing activity, and thus translational infidelity, are dependent on the cell type and the extent of editing disruption, and provide a previously unidentified mechanism underlying cardiac proteinopathy.

translational fidelity | mistranslation | protein misfolding | protein quality control | cardiomyopathy

Proteins are the building blocks and major signaling molecules of cells, and as such, their synthesis and degradation are tightly regulated. Disruption of protein homeostasis (proteostasis) can result in the accumulation of abnormal proteins that lead to cellular pathogenesis. Like the neuroproteopathies, misfolding of specific proteins in cardiomyocytes can be caused by genetic mutations that alter the primary structure of aggregated proteins. For example, mutations in the desmin gene, which encodes a muscle-specific intermediate filament protein, or in the gene encoding αB-crystallin, a molecular chaperone for desmin, result in aggregation of these proteins and are a primary cause of hereditary cardiomyopathy (1, 2). Systemic amyloidosis, the extracellular accumulation of abnormal proteinaceous fibrils, can also occur in the heart with detrimental effects on cardiac function (3, 4). In addition, misfolded proteins and changes in the ubiquitin proteasome system or autophagy have been widely reported in failing hearts (4, 5), demonstrating the importance of protein quality control systems for cardiomyocyte homeostasis. However, whether such proteostatic changes induce pathological changes, or are consequences of the diseased state, is not clear.

In addition to genetic mutations, defective proteins can be generated by inaccurate translation. Translational fidelity is largely controlled by the precise aminoacylation of tRNAs with their cognate amino acids, a function carried out by the aminoacyl-tRNA synthetases (aaRSs). To improve substrate specificity, an editing site, which hydrolyses misactivated noncognate amino acids or mischarged tRNAs and is distinct from the aminoacylation domain, is found in approximately half of the aaRSs (6, 7). Failure of proofreading by these aaRSs may result in incorporation of the wrong amino acid into the nascent peptide, which could be detrimental to protein folding and function.

Although errors in aminoacylation are relatively low (8, 9), even small decreases in aaRS proofreading have dramatic effects on cell survival (10–12). Bacterial alanyl-tRNA synthetase (AlaRS) can misactivate glycine or serine, and *Escherichia coli* expressing a severe editing-deficient form (C666A) of AlaRS had increased death when grown in elevated concentrations of these amino acids (11). In mice, a point mutation (A734E) in the AlaRS editing domain in the mutant strain "sticky" caused a twofold increase in Ser-mischarged $tRNA^{Ala}$ that resulted in formation of ubiquitinated protein aggregates in cerebellar Purkinje cells and degeneration of these neurons (10). However, because cell loss in other regions of the brain or in other tissues was not observed in the *sti* mutant mouse, the importance of AlaRS editing activity in other mammalian cell types remains unknown.

Here we hypothesized that further decreases in AlaRS editing function could lead to misfolded protein accumulation in additional cell types. Indeed mouse embryos homozygous for a point mutation at C723 (which corresponds to the C666 amino acid in the editing domain of bacterial AlaRS) died by midgestation. Furthermore, decreasing the amount of the *sti*-associated $AlaRS^{A734E}$ enzyme or placing the *sti* mutation and the more severe AlaRS ($Aars^{C723A}$) mutation in *trans* caused extensive aggregation of misfolded proteins in mouse cardiomyocytes, eventually leading to cardiomyopathy. Using this proteome-wide mistranslation system, we demonstrate that different cell types are distinctly sensitive to errors in protein synthesis and that mistranslation can induce

Significance

Misfolded proteins are a hallmark of diverse human cardiac disorders including desmin-related cardiomyopathy and systemic amyloidosis. Defects in translational fidelity can cause neurodegeneration, however the consequences of mistranslation in other tissues, including the heart, are unknown. The fidelity of protein synthesis is largely ensured by aminoacyl-tRNA synthetases, and many tRNA synthetases contain editing domains that hydrolyze mischarged tRNAs, preventing incorporation of incorrect amino acids into proteins. Here, we show that diminished editing efficacy of the alanyl-tRNA synthetase causes misfolded protein aggregation and cell death in the mammalian heart. These results illuminate the importance of translational fidelity in cardiac homeostasis and suggest that genetic factors that disrupt the accuracy of translation may contribute to proteinopathies of the heart and other tissues.

Author contributions: Y.L., J.S.S., M.-N.V., L.A.N., P.S., and S.L.A. designed research; Y.L., J.S.S., M.-N.V., and L.A.N. performed research; Y.L., J.S.S., M.-N.V., L.A.N., P.S., and S.L.A. analyzed data; and Y.L., J.S.S., M.-N.V., L.A.N., P.S., and S.L.A. wrote the paper.

The authors declare no conflict of interest.

[1]Present address: aTyr Pharma Inc., San Diego, CA 92121.

[2]To whom correspondence may be addressed. Email: schimmel@scripps.edu or susan.ackerman@jax.org.

This article contains supporting information online at www.pnas.org/lookup/suppl/doi:10.1073/pnas.1420196111/-/DCSupplemental.

cardiac proteinopathy, which leads to cardiac fibrosis and decrements in heart function.

Results

Previous results determined that Cys666 in the editing domain of bacterial AlaRS was essential for AlaRS editing (11). In agreement, mutation of Cys723 (corresponding to bacterial Cys666) to Ala in mammalian AlaRS resulted in a dramatic increase in production of mischarged Ser-tRNA^{Ala} (Fig. 1*A*, *Left*). In contrast to the twofold increase in mischarged Ser-tRNA^{Ala} generated by AlaRS^{A734E}, the mutant enzyme found in *sti* mutant mice (10), in vitro misacylation assays demonstrated that the C723A enzyme produced Ser-tRNA^{Ala} at initial rates at least 15-fold higher than that produced by the wild-type enzyme.

To determine the in vivo effects of this dramatic loss in AlaRS editing activity, the C723A mutation was introduced into the mouse *Aars* gene via homologous recombination (Fig. 1*B*). To achieve conditional expression of the knock-in allele, a loxP-flanked transcriptional stop cassette (13, 14) was also inserted in intron 1 of this gene. Constitutive expression of *Aars*^{C723A} was induced by crossing *Aars*$^{stop/+}$ mice to the EIIa-Cre strain to remove the stop cassette (15). The resulting *Aars*$^{C723A/+}$ offspring were viable and indistinguishable from wild-type littermates. We hypothesized that wild-type AlaRS in the *Aars*$^{C723/+}$ mouse could edit in *trans* the Ser-tRNA^{Ala} produced by C723A AlaRS. An in vitro mixing of C723A AlaRS with wild-type AlaRS confirmed this expectation (Fig. 1*A*, *Right*).

Still, careful examination of brains from aged *Aars*$^{C723A/+}$ mice revealed mild loss of cerebellar Purkinje cells (Fig. S1). This minor neuronal loss could result from the ability of eukaryotic translation elongation factor 1 alpha to capture some of the mischarged tRNA and prevent its clearance by wild-type AlaRS (10). In comparison, Purkinje cell loss is not observed in aged *Aars*$^{sti/+}$ mice, and *Aars*$^{sti/sti}$ mice have early onset and severe Purkinje cell degeneration (10). Moreover, no abnormalities were observed in brain regions other than the cerebellum or in other organs (*SI Materials and Methods*) from 10- to 18-mo-old *Aars*$^{C723A/+}$ mice (Fig. S1). Together these observations suggest that due to the further reduction in AlaRS editing activity, the effects of the *Aars*^{C723A} mutation are more detrimental than the *Aars*^{sti} mutation in vivo. Consistent with this notion, no *Aars*$^{C723A/C723A}$ offspring were obtained from *Aars*$^{C723A/+}$ intercrosses, demonstrating that homozygous expression of this mutation was lethal (Table S1). In addition, no viable E8.5/E9.5

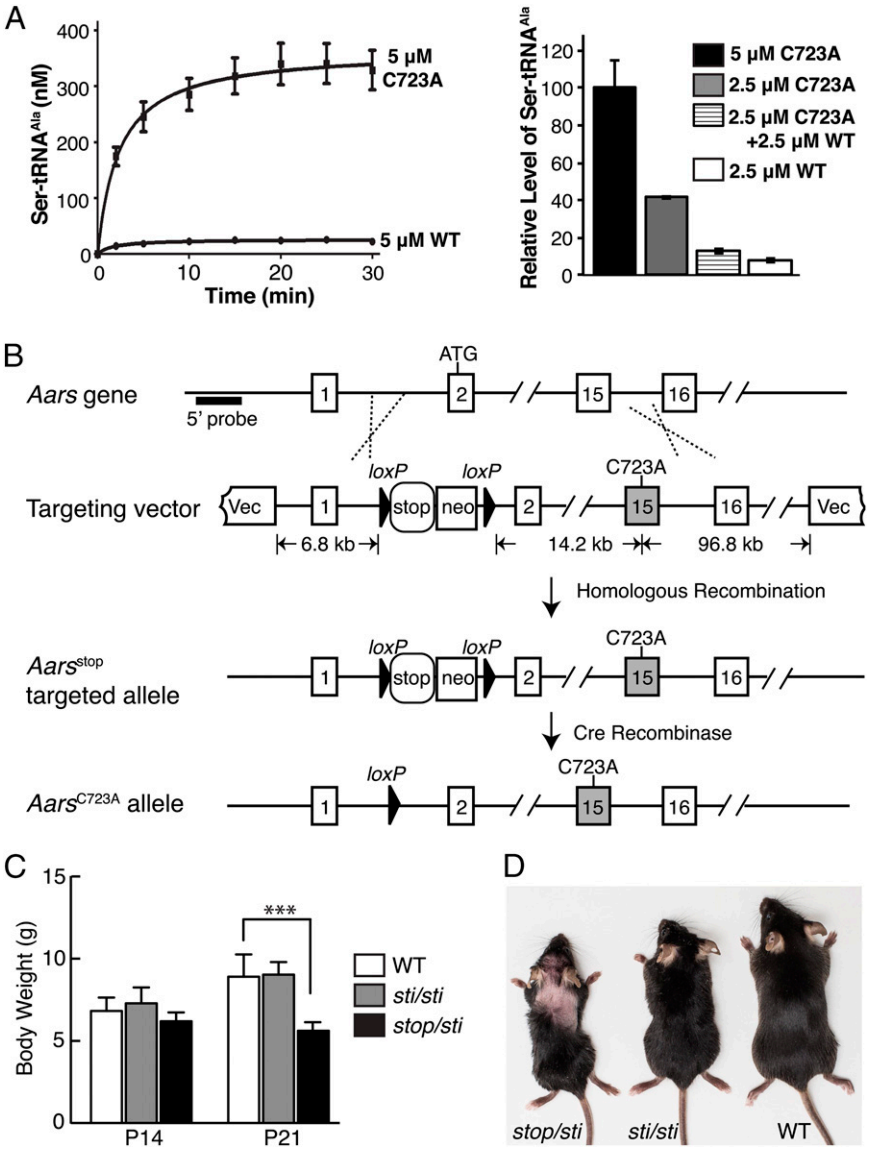

Fig. 1. Generation of editing-defective AlaRS mouse models. (*A*, *Left*) Misacylation of tRNA^{Ala} with serine by mouse wild-type (WT) or C723A AlaRS. (*Right*) Relative level of mischarged Ser-tRNA^{Ala} in the presence of WT, C723A, or equal molar ratio of WT and C723A AlaRS at 15 min. Assays were run in duplicate, and points (mean ± SD) were averaged from two experiments. (*B*) To generate the conditional knock-in allele of AlaRS^{C723A}, a loxP-flanked transcriptional stop cassette was inserted in intron 1, and the TGT codon encoding cysteine at position 723 in exon 15 was replaced with a GCG alanine codon. *Aars* transcription remains off until the stop cassette is deleted via Cre expression. The Southern blot probe (5′ probe), the size of the left and right "arm" of the targeting vector, and the distance between the neo cassette and exon 15 are indicated. (*C*) Body weight of WT (n = 13), *Aars*$^{sti/sti}$ (*sti/sti*; n = 8), and *Aars*$^{stop/sti}$ (*stop/sti*; n = 11) mice at postnatal ages (P) 14 and P21. Values represent mean ± SD; ***P < 0.0001 (one-way ANOVA). (*D*) Photograph of 2-mo-old WT, *Aars*$^{sti/sti}$, and *Aars*$^{stop/sti}$ mice. Note the dorsal alopecia characteristic of the *Aars*$^{stop/sti}$ mouse.

Aars$^{C723A/C723A}$ embryos were observed, and 26% (n = 9/34) of decidua at these time points contained embryos that were too reabsorbed for genotyping, suggesting that the homozygous embryos died at an earlier stage of development (Table S1). These results, compared with our previous findings of neuron-specific defects in the *sti* mutant mouse (10), indicate that the *Aars*^{C723A} mutation likely causes a higher rate of translational errors in vivo than the *sti* mutation and that phenotypes caused by deficiencies in AlaRS editing are dependent on the extent of the residual editing activity of the mutant enzyme.

To create a mouse model with an editing deficiency between that of *Aars*$^{C723A/C723A}$ and *Aars*$^{sti/sti}$ mice, we generated *Aars*$^{stop/sti}$ compound heterozygotes. These mice were viable and present at weaning age in the expected Mendelian ratios. Although initially indistinguishable from wild-type littermates, at 3 wk of age *Aars*$^{stop/sti}$ mice were smaller than wild-type or *Aars*$^{sti/sti}$ mice (Fig. 1*C*). In addition, larger regions of alopecia were consistently observed in *Aars*$^{stop/sti}$ than in *Aars*$^{sti/sti}$ mice (Fig. 1*D*). The gene dosage effect of the *Aars*^{sti} mutation reinforces the notion that cells differ in their sensitivity to disruptions in translational fidelity.

Histological analysis of the *Aars*$^{stop/sti}$ brain demonstrated that the temporal and spatial pattern of Purkinje cell degeneration was very similar to that observed in *Aars*$^{sti/sti}$ mice (Fig. S1). However, gross morphological examination of other tissues from 10-mo-old mice revealed that the heart of *Aars*$^{stop/sti}$ mice was smaller than those from age-matched *Aars*$^{sti/sti}$ or wild-type mice (Fig. 2 *A* and *B*). Although histological analysis of other organs did not reveal abnormalities, myofiber disarray was observed in the ventricular myocardium of hearts from *Aars*$^{stop/sti}$ mice. Masson's trichrome and picrosirius red staining of sections from 4- and 10-mo-old *Aars*$^{stop/sti}$ mice revealed extensive fibrosis, which typically forms where cardiomyocytes have degenerated. Both interstitial and perivascular fibrosis was observed in the left and right ventricular walls and in the interventricular septum (IVS) of affected hearts (Fig. 2 *C* and *D* and Fig. S2). Moreover, the development of cardiac fibrosis in the *Aars*$^{stop/sti}$ mouse appeared to be age-related: At 1 mo of age, no apparent fibrosis was observed in heart sections; at 4 mo of age, ~2.5% of the heart tissue was fibrotic; and by 10 mo of age, fibrotic areas increased to about 7.5% of the *Aars*$^{stop/sti}$ heart (Fig. 2*G*). In contrast, no fibrotic lesions were observed in 10-mo-old *Aars*$^{sti/sti}$ or wild-type mice (Fig. 2 *E*–*G*).

In an alternative effort to diminish the editing activity of the AlaRS enzyme in vivo, we generated *Aars*$^{C723A/sti}$ mice. Similar to *Aars*$^{stop/sti}$ mice, these mice were smaller than *Aars*$^{sti/sti}$ mice, with larger regions of dorsal alopecia. In addition, widespread myocardial fibrosis was present in the hearts of 4-mo-old *Aars*$^{C723A/sti}$ mice (Fig. S3), confirming that editing activity in between that of AlaRS^{A734E} or AlaRS^{C723A} results in death of cardiomyocytes.

Fibrotic cardiac muscle is stiffer and less compliant than normal heart muscle and is commonly associated with cardiac failure (16). To determine if fibrosis affected the contractile function of the *Aars*$^{stop/sti}$ heart, echocardiography was performed on 10-mo-old *Aars*$^{stop/sti}$, *Aars*$^{sti/sti}$, and wild-type mice (Fig. S4 and Table S2). Echocardiogram parameters revealed that the *Aars*$^{stop/sti}$ mutant heart exhibited a slight, but significant, reduction in the thickness of the left ventricular posterior wall. Although not significant, the *Aars*$^{stop/sti}$ septum also tended to be thinner than that of wild-type mice (IVSs). Consistent with the observed pathology, less systolic thickening of the left ventricle was seen in the *Aars*$^{stop/sti}$ heart, indicating myocardial dysfunction. Furthermore, ventricular output, as measured by the ejection fraction and fractional shortening of the left ventricle, was significantly reduced in *Aars*$^{stop/sti}$ but not *Aars*$^{sti/sti}$ or *Aars*$^{C723A/+}$ mice (Fig. 2*H* and Fig. S1).

Electrophysiological function of *Aars*$^{stop/sti}$ and *Aars*$^{sti/sti}$ hearts was further evaluated by electrocardiogram telemetry in 10-mo-old

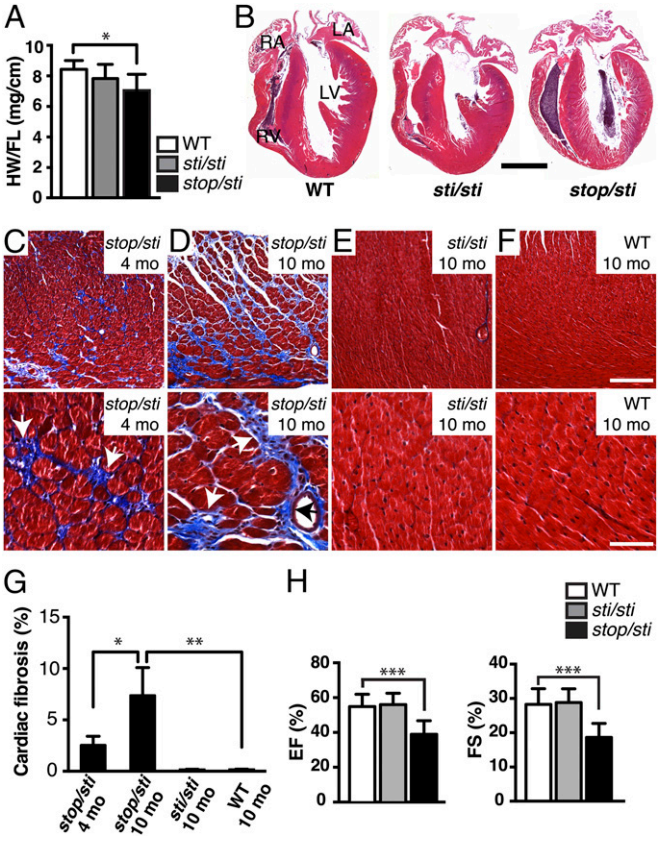

Fig. 2. Cardiac abnormalites in *Aars*$^{stop/sti}$ mice. (*A*) Ratio of the heart weight to femur length (HW/FL) from 10-mo-old WT (n = 11), *Aars*$^{sti/sti}$ (*sti/sti*; n = 6), and *Aars*$^{stop/sti}$ (*stop/sti*; n = 8) mice. Values represent mean ± SD; *P < 0.01 (one-way ANOVA). (*B*) Hematoxylin and eosin staining of longitudinal sections of hearts from 10-mo-old mice with the indicated genotypes. (Scale bar, 2 mm.) (*C*–*F*) Masson's trichrome stain of heart sections from 4- (*C*) and 10-mo-old (*D*) *Aars*$^{stop/sti}$ and 10-mo-old *Aars*$^{sti/sti}$ (*E*) and WT (*F*) mice. Higher magnification photos of a representative area of each image are shown in the *Lower* panel. Note the high levels of interstitial fibrosis (blue; white arrows) and perivascular fibrosis (blue; black arrows) in *Aars*$^{stop/sti}$ but not *Aars*$^{sti/sti}$ or WT hearts. (Scale bars, 200 μm and 60 μm for the *Upper* and *Lower* panel, respectively.) (*G*) Quantification of fibrotic areas (as a percentage of total area). Values are mean ± SD; *P < 0.01 (unpaired t test) and **P < 0.001 (one-way ANOVA); n = 4 mice for each data point. (*H*) Ejection fraction (EF%; *Left* graph) and fractional shortening (FS%; *Right* graph) of 10-mo-old WT (n = 15), *Aars*$^{sti/sti}$ (n = 6), and *Aars*$^{stop/sti}$ (n = 9) mice. Values are mean ± SD; ***P < 0.0001 (one-way ANOVA).

mice. Electrocardiographic characteristics were similar between different genotypes, and ventricular arrhythmias were not observed in any mice (Fig. S5).

Previously we showed that accumulation of misfolded proteins in *Aars*$^{sti/sti}$ Purkinje cells accompanied their degeneration (10). To determine whether similar mechanisms occurred in *Aars*$^{stop/sti}$ cardiomyocytes, ubiquitin immunofluorescence was performed on heart sections of 10-mo-old mutant and wild-type mice (Fig. 3*A*). In the wild-type heart, ubiquitin signals were present in the cytoplasm and in the nucleus, as previously reported (17). However, ubiquitin-positive puncta characteristic of protein aggregates were not detected in the wild-type heart. In contrast, ubiquitin puncta were present in ~2.4% of cardiomyocytes in *Aars*$^{stop/sti}$ hearts (n = 4). In addition, large vacuoles and a reduction in fiber diameter were often observed in aggregate-containing cardiomyocytes, consistent with cellular atrophy and cell death (Fig. 3*A*).

To determine the onset of proteinopathy in mutant cardiomyocytes, ubiquitin immunofluorescence was performed on

hearts from younger *Aars*$^{stop/sti}$ mice. At 1 mo of age, most cardiomyocytes in *Aars*$^{stop/sti}$ hearts appeared normal, with cells containing ubiquitinated aggregates only occasionally observed. However, the number of aggregate-containing cells drastically increased by 2 mo of age, constituting ∼1.8% of total cells in the *Aars*$^{stop/sti}$ heart. In comparison, cardiomyocytes of *Aars*$^{sti/sti}$ mice appeared normal, and ubiquitin-positive inclusions were rarely observed at any given age. Our observations that protein aggregates occurred in prefibrotic *Aars*$^{stop/sti}$ hearts and that the number of cardiomyocytes with aggregates increased with age suggest that misfolded proteins induce cardiomyocyte death.

In addition to the ubiquitin–proteasome protein degradation pathway, aggregates of ubiquitinated proteins can be degraded by autophagy. Thus, autophagy is often up-regulated as an adaptive response to the increased production of misfolded proteins. Correspondingly, suppression of autophagy in diseased hearts leads to cardiomyopathy (5). The autophagic adapter protein p62/sequestosome 1 noncovalently interacts with ubiquitinated proteins through its C-terminal domain and facilitates their degradation via autophagy (18, 19). Recent studies demonstrate that p62 is often associated with aggresomes in desmin-associated cardiomyopathies (5, 20). Coimmunofluorescence using antibodies to p62 and ubiquitin in 2-mo-old *Aars*$^{stop/sti}$ hearts demonstrated that the majority of ubiquitinated aggregates also contained p62 (Fig. 3*B*). Ubiquitin and p62-positive puncta were also observed in cardiomyocytes of *Aars*$^{C723A/sti}$ mice, further demonstrating the convergence of the two mouse models (Fig. S3).

Immunofluorescence with antibodies to microtubule-associated protein 1 light chain 3 (LC3), a marker of autophagosomes, on sections of *Aars*$^{stop/sti}$ hearts also showed colocalization of LC3 and protein aggregates (Fig. 3*C*). In addition, coimmunofluorescence with antibodies to stress-inducible Hsp70, a molecular chaperone often colocalized with intracellular inclusions (21, 22), revealed colocalization of p62-positive aggregates with Hsp70, further confirming that these structures contain misfolded or unfolded proteins (Fig. 3*D*). Lastly, because AlaRS editing defects have the potential to cause mistranslation of any protein containing alanine, we determined if protein aggregates in *Aars*$^{stop/sti}$ hearts contained desmin, previously shown to form aggregates in the genetic desminopathy disorders (23). In both wild-type and *Aars*$^{stop/sti}$ hearts, desmin was detected at the sarcomeric Z-disk (Fig. S6). However, no colocalization of p62 and desmin was observed in the *Aars*$^{stop/sti}$ heart, suggesting desmin is not a major component of protein aggregates.

We further performed transmission electron microscopy that revealed multiple pathological changes in *Aars*$^{stop/sti}$ cardiomyocytes. Consistent with our immunofluorescence observations, deposition of protein aggregates that disrupt myofibrillar structure was observed in mutant, but not wild-type, cardiomyocytes (Fig. 4*A*). In addition, many mutant cardiomyocytes had abnormal accumulation of autophagic vacuoles of different stages, indicative of elevated autophagy (Fig. 4 *B* and *C*). Multilamellar bodies indicative of impaired lysosomal degradation of autophagic cargos (24) were apparent in mutant, but not wild-type, cells (Fig. 4 *D*–*F*), suggesting that autophagic clearance is likely compromised in *Aars*$^{stop/sti}$ mutant cells. In addition to accumulation of autophagic structures, we observed abnormal mitochondria and disruption of the sarcoplasmic reticulum in mutant cardiomyocytes (Fig. 4 *B*, *G*, and *H*). These pathological changes may reflect the toxic effects of misfolded proteins and may contribute to degeneration of cardiomyocytes.

Discussion

The effect of mistranslation on the cellular homeostasis of complex higher organisms remains poorly understood. To explore the pathological impact of increased translational errors in vivo, we genetically decreased the editing function of the mouse AlaRS enzyme. This decrease in editing in turn affects global translation by increasing the incorporation of noncognate amino acids into nascent proteins. Our "fine-tuning" of the editing efficiency of AlaRS demonstrated that the severity of the resulting phenotypes directly correlated with the residual editing activity of the enzyme. The originally identified *Aars*^{sti} (A734E) mutation is the mildest allele in our series. Homozygosity for this mutation selectively induces protein aggregation and apoptosis in cerebellar Purkinje cells (10). In contrast, embryos homozygous for the *Aars*^{C723A} allele, which causes dramatic increases in mischarged Ser-tRNA^{Ala}, died before midgestation, suggesting that editing activity is essential for mammalian development. Interestingly, mice that were heterozygous for the *Aars*^{C723A} mutation were largely phenotypically normal, with only loss of a minor population of Purkinje cells in aged mice. This finding indicates that AlaRS expressed from the wild-type allele is sufficient in *trans* to hydrolyze the Ser-tRNA^{Ala} generated by the mutant enzyme. Further genetic regulation of the editing efficacy of the *Aars*^{sti} allele by either lowering the level of the enzyme (as in *Aars*$^{stop/sti}$ mice) or placing the *Aars*^{sti} allele over the *Aars*^{C723A} mutation resulted in phenotypes intermediate to those in *Aars*$^{sti/sti}$ and *Aars*$^{C723A/C723A}$ mice, including loss of Purkinje cells and widespread protein aggregate formation in cardiomyocytes and

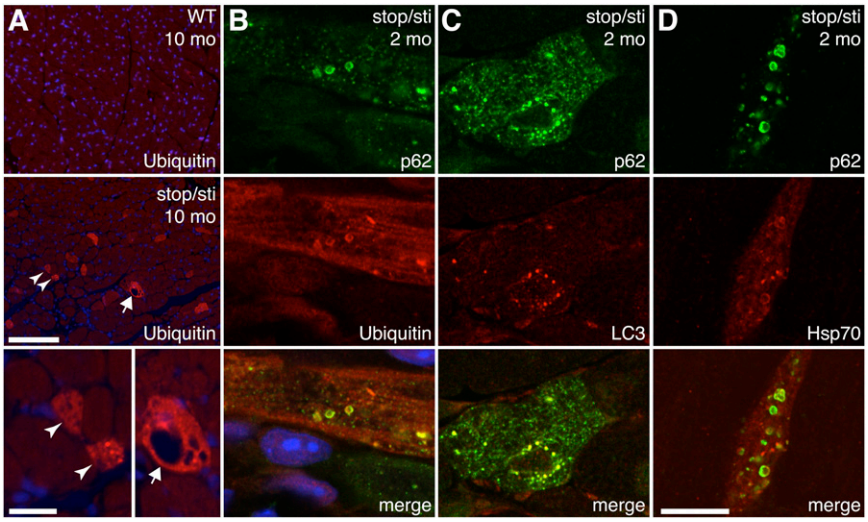

Fig. 3. Formation of misfolded protein aggregates in *Aars*$^{stop/sti}$ mutant cardiomyocytes. (*A*) Immunofluorescence with antibodies to ubiquitin on heart sections from 10-mo-old WT and *Aars*$^{stop/sti}$ mice. Nuclei are counterstained with Hoechst dye (blue). Higher magnification photos of *Aars*$^{stop/sti}$ cardiomyocytes are shown in the *Lower* panel. Arrowheads indicate myofibers with intense ubiquitin signals and reduced fiber diameter. An arrow indicates a cardiomyocyte with elevated ubiquitin and vacuoles. (*B*–*D*) High-magnification confocal microscopic images showing colocalization of p62 with ubiquitin (*B*), LC3 (*C*), and Hsp70 (*D*) within the cytoplasm of representative cardiomyocytes of 2-mo-old *Aars*$^{stop/sti}$ mice. [Scale bars, (*A*, *Upper* and *Middle* panels) 100 μm, (*A*, *Lower* panel) 20 μm, and (*B*–*D*) 10 μm.]

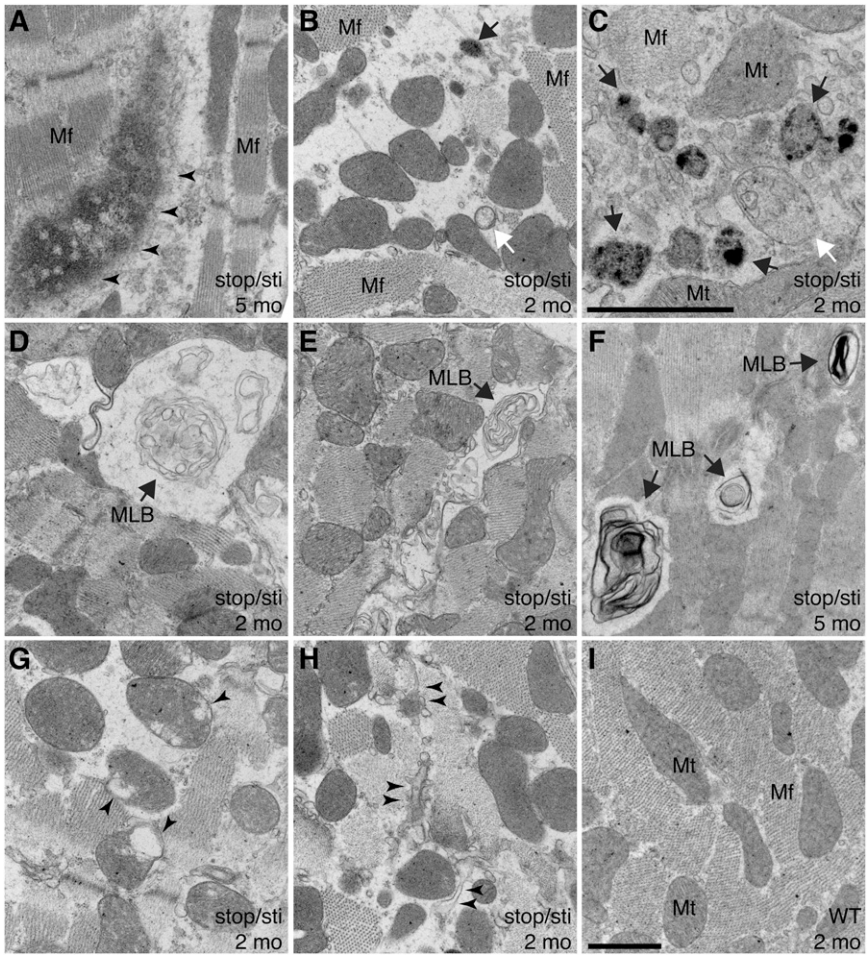

Fig. 4. Ultrastructural changes in *Aars*$^{stop/sti}$ cardiomyocytes. (*A–I*) Representative transmission electron microscope images of hearts from 2-mo- (*B–E*, *G*, and *H*) and 5-mo-old (*A* and *F*) *Aars*$^{stop/sti}$ mice and 2-mo-old WT (*I*) mice. (*A*) Formation of large protein aggregates (arrowheads) that disrupt myofibril (Mf) structures. (*B* and *C*) Accumulation of autophagic vacuoles (white arrow, early autophagosome; black arrow, autolysosome) accompanied by loss of Mf structures. (*D–F*) Multilamellar bodies (MLBs, arrows), products of active autophagy and a hallmark of insufficient lysosomal activity, are also present. (*G*) Defective mitochondria (Mt) with disrupted cristae (arrowheads). (*H*) Disrupted sarcoplasmic reticulum (arrowheads) in *Aars*$^{stop/sti}$ cardiomyocytes. [Scale bars, (*A*, *B*, and *D–I*) 1 μm and (*C*) 1 μm.]

subsequent death of these cells. These results suggest that the response to mistranslation varies among cells and that protein aggregates may be induced in additional cell types upon further decreases in translational fidelity.

Our results define a common mechanism of protein aggregation in cardiomyocytes and neurons. The underlying sensitivity of these two cell types to mistranslation may lie in the postmitotic nature of these cells, in which protein aggregates are not diluted by cell division (25). Moreover, hydrolysis of misacylated tRNA may be subject to additional regulation. Indeed, Ser-tRNA^{Ala} can also be hydrolyzed by a free-standing editing domain protein, *Aarsd1* (AlaXP) (26, 27), which could compensate for editing deficiencies in AlaRS. Lastly, the differential sensitivity of cells to translation errors may be due to the varying capacity of protein quality control systems in different cell types.

Although decreased translation fidelity causes protein misfolding and aggregation in both cardiomyocytes and Purkinje cells, the downstream pathways that lead to cell death in the two cell types may be quite different. Purkinje cells in sticky mutant mice undergo apoptosis (10), whereas cardiomyocytes in the *Aars*$^{stop/sti}$ mouse were negative for cleaved caspase 3 and TUNEL labeling. In addition, abnormal mitochondria with disorganized cristae that may be a contributing factor in cell death were observed in *Aars*$^{stop/sti}$ cardiomyocytes. Interestingly, a point mutation in the editing domain of human mitochondrial AlaRS (*AARS2*) has been associated with infantile mitochondrial cardiomyopathy (28), suggesting increased errors in either cytoplasmic or mitochondrial protein synthesis can lead to cell death in the heart.

In summary, our data show that a global reduction in translational fidelity, rather than disruption of a specific protein, can induce defects in proteostasis in numerous cell types in the mouse. Indeed, fidelity of protein synthesis is not only subjected to genetic changes that modulate translation machinery, it can also be affected by environmental factors such as oxidative stress. The cysteine 182 residue that is critical for editing activity of threonyl-tRNA synthetase in *E. coli* can be oxidized by reactive oxygen species, and thus, overall translational fidelity is impaired as a result (29). In mammalian cells, various environmental factors that trigger oxidative stress are known to increase Met-misacylation of tRNAs (30). It is thus possible that proteinopathy can occur in the brain, heart, or even other tissues as a combination of genetic and/or environmental factors that compromise translational fidelity.

Materials and Methods

Misacylation Assays. Misacylation assays were performed with mouse wild-type or mutant C723A AlaRS, 10 μM ^{3}H-L-serine, and 10 μM human tRNA^{Ala} following methods described in ref. 31. Overexpression and purification of

human $tRNA^{Ala}$ was performed as previously described (10). Details are provided in *SI Materials and Methods*.

Mice. All animal protocols were approved by The Jackson Laboratory Animal Care and Use Committee. Homologous recombination of the $Aars^{stop}$ allele was performed in C57BL/6J-Tyr^{c-2J} ES cells. $Aars^{sti/sti}$ and Tg(EIIa-cre) C5379Lmgd/J mice were maintained on a C57BL/6 genetic background (10, 15). Generation of the knock-in mouse and genotyping information are described in *SI Materials and Methods*.

Echocardiography and Electrocardiography. Cardiac function, heart dimensions, and electrical activity of the heart were evaluated by echocardiography and electrocardiography on anesthetized mice. Details are provided in *SI Materials and Methods*.

Histology. Hematoxylin and eosin, Masson's trichrome, and picrosirius red staining was performed on 10% (vol/vol) neutral buffered formalin (NBF)-fixed tissue sections. Details are described in *SI Materials and Methods*.

Immunofluorescence. The 10% NBF-fixed, paraffin-embedded heart sections were deparaffinated, rehydrated, and microwaved in 0.01 M citrate buffer (pH 6.0) three times for 2 min each. Tissue sections were then blocked with 4% (wt/vol) goat serum in phosphate-buffered saline with Tween-20 (PBST) for 30 min, incubated with primary antibodies overnight at 4 °C, washed in PBST, and incubated with secondary antibodies for 1 h. Details about antibodies are described in *SI Materials and Methods*.

Electron Microscopy. Mice were transcardially perfused with 2% (wt/vol) paraformaldehyde and 2% (wt/vol) glutaraldehyde. Tissues were prepared for analysis using standard procedures.

Statistics. Results are mean ± SD. Statistical significance was determined by unpaired *t* tests or one-way ANOVA followed by Dunnett's multiple-comparisons test. *P* values less than 0.05 were considered significant.

ACKNOWLEDGMENTS. We are grateful to Jennifer Cook and Krystal-Leigh Baker for technical assistance, Litao Sun for $tRNA^{Ala}$, Jennifer Ryan for ECG and echocardiography recordings, Mark Lessard for help with imaging and quantification, Pete Finger for electron microscopy assistance, and Doug McMinimy for mouse photos. We also thank Dr. Karen Svenson for helpful discussions, Dr. Greg Cox for comments on the manuscript, and The Jackson Laboratory sequencing, histology, and microinjection services for their contributions. These studies were supported by National Institutes of Health Grant NS042613 (to S.L.A.), and services used in this study were supported by Cancer Center Core Grant CA34196 (The Jackson Laboratory). Support was also provided by aTyr Pharma, Inc., The National Foundation for Cancer Research, and National Cancer Institute Grant CA92577. J.S.S. was supported by a fellowship from the American Health Assistance Foundation. S.L.A. is an investigator of the Howard Hughes Medical Institute.

1. Goldfarb LG, Dalakas MC (2009) Tragedy in a heartbeat: Malfunctioning desmin causes skeletal and cardiac muscle disease. *J Clin Invest* 119(7):1806–1813.
2. McLendon PM, Robbins J (2011) Desmin-related cardiomyopathy: An unfolding story. *Am J Physiol Heart Circ Physiol* 301(4):H1220–H1228.
3. Quarta CC, Kruger JL, Falk RH (2012) Cardiac amyloidosis. *Circulation* 126(12): e178–e182.
4. Wang X, Robbins J (2006) Heart failure and protein quality control. *Circ Res* 99(12): 1315–1328.
5. Zheng Q, Su H, Ranek MJ, Wang X (2011) Autophagy and p62 in cardiac proteinopathy. *Circ Res* 109(3):296–308.
6. Ling J, Reynolds N, Ibba M (2009) Aminoacyl-tRNA synthesis and translational quality control. *Annu Rev Microbiol* 63:61–78.
7. Schimmel P (2008) Development of tRNA synthetases and connection to genetic code and disease. *Protein Sci* 17(10):1643–1652.
8. Loftfield RB, Vanderjagt D (1972) The frequency of errors in protein biosynthesis. *Biochem J* 128(5):1353–1356.
9. Jakubowski H, Goldman E (1992) Editing of errors in selection of amino acids for protein synthesis. *Microbiol Rev* 56(3):412–429.
10. Lee JW, et al. (2006) Editing-defective tRNA synthetase causes protein misfolding and neurodegeneration. *Nature* 443(7107):50–55.
11. Beebe K, Ribas De Pouplana L, Schimmel P (2003) Elucidation of tRNA-dependent editing by a class II tRNA synthetase and significance for cell viability. *EMBO J* 22(3): 668–675.
12. Nangle LA, Motta CM, Schimmel P (2006) Global effects of mistranslation from an editing defect in mammalian cells. *Chem Biol* 13(10):1091–1100.
13. Soriano P (1999) Generalized lacZ expression with the ROSA26 Cre reporter strain. *Nat Genet* 21(1):70–71.
14. Srinivas S, et al. (2001) Cre reporter strains produced by targeted insertion of EYFP and ECFP into the ROSA26 locus. *BMC Dev Biol* 1:4.
15. Lakso M, et al. (1996) Efficient in vivo manipulation of mouse genomic sequences at the zygote stage. *Proc Natl Acad Sci USA* 93(12):5860–5865.
16. Weber KT, Brilla CG, Janicki JS (1993) Myocardial fibrosis: Functional significance and regulatory factors. *Cardiovasc Res* 27(3):341–348.
17. Hilenski LL, Terracio L, Haas AL, Borg TK (1992) Immunolocalization of ubiquitin conjugates at Z-bands and intercalated discs of rat cardiomyocytes in vitro and in vivo. *J Histochem Cytochem* 40(7):1037–1042.
18. Vadlamudi RK, Joung I, Strominger JL, Shin J (1996) p62, a phosphotyrosine-independent ligand of the SH2 domain of p56lck, belongs to a new class of ubiquitin-binding proteins. *J Biol Chem* 271(34):20235–20237.
19. Pankiv S, et al. (2007) p62/SQSTM1 binds directly to Atg8/LC3 to facilitate degradation of ubiquitinated protein aggregates by autophagy. *J Biol Chem* 282(33):24131–24145.
20. Olivé M, et al. (2008) Expression of mutant ubiquitin (UBB+1) and p62 in myotilinopathies and desminopathies. *Neuropathol Appl Neurobiol* 34(1):76–87.
21. Warrick JM, et al. (1999) Suppression of polyglutamine-mediated neurodegeneration in Drosophila by the molecular chaperone HSP70. *Nat Genet* 23(4):425–428.
22. Waelter S, et al. (2001) Accumulation of mutant huntingtin fragments in aggresome-like inclusion bodies as a result of insufficient protein degradation. *Mol Biol Cell* 12(5): 1393–1407.
23. Clemen CS, Herrmann H, Strelkov SV, Schröder R (2013) Desminopathies: Pathology and mechanisms. *Acta Neuropathol* 125(1):47–75.
24. Hariri M, et al. (2000) Biogenesis of multilamellar bodies via autophagy. *Mol Biol Cell* 11(1):255–268.
25. Soonpaa MH, Field LJ (1997) Assessment of cardiomyocyte DNA synthesis in normal and injured adult mouse hearts. *Am J Physiol* 272(1 Pt 2):H220–H226.
26. Nawaz MH, Merriman E, Yang XL, Schimmel P (2011) p23H implicated as cis/trans regulator of AlaXp-directed editing for mammalian cell homeostasis. *Proc Natl Acad Sci USA* 108(7):2723–2728.
27. Chong YE, Yang XL, Schimmel P (2008) Natural homolog of tRNA synthetase editing domain rescues conditional lethality caused by mistranslation. *J Biol Chem* 283(44): 30073–30078.
28. Götz A, et al. (2011) Exome sequencing identifies mitochondrial alanyl-tRNA synthetase mutations in infantile mitochondrial cardiomyopathy. *Am J Hum Genet* 88(5): 635–642.
29. Ling J, Söll D (2010) Severe oxidative stress induces protein mistranslation through impairment of an aminoacyl-tRNA synthetase editing site. *Proc Natl Acad Sci USA* 107(9):4028–4033.
30. Netzer N, et al. (2009) Innate immune and chemically triggered oxidative stress modifies translational fidelity. *Nature* 462(7272):522–526.
31. Beebe K, Waas W, Druzina Z, Guo M, Schimmel P (2007) A universal plate format for increased throughput of assays that monitor multiple aminoacyl transfer RNA synthetase activities. *Anal Biochem* 368(1):111–121.